PAPER

Check for updates

Silver decorated on cobalt ferrite nanoparticles as a reusable multifunctional catalyst for water treatment applications in non-radiation conditions

Le Thi Ngoc Hoa,[†abc] Vu Nang An, [ID] [†ab] Vo Huynh Tra My,[ab] Pham Thi Thu Giang,[ab] Le Khac Top,[ab] Ha Thuc Chi Nhan,[ab] Phan Bach Thang, [ID] [bd] Tran Thi Thanh Van [ID] [ab] and Le Van Hieu [ID] [*abc]

In this investigation, cobalt ferrite nanoparticles (CFO NPs) were synthesized using a hydrothermal method. Then, silver nanoparticles (Ag NPs) were decorated on CFO NPs to form Ag/CFO NPs using jasmine extract as a reducing agent of Ag^+ ions. The properties of Ag/CFO NPs were characterized by X-ray powder diffraction, field-emission scanning electron microscopy, energy-dispersive X-ray spectroscopy, Fourier-transform infrared spectroscopy, vibrating sample magnetometry, and catalytic tests in non-radiation conditions. The catalytic results indicated that the Ag/CFO NPs could activate peroxymonosulfate to generate sulfate radicals for the decomposition of different dyes such as methylene blue, methyl orange, and rhodamine B. For the Ag/CFO sample, Ag NPs validated the roles in dye adsorption, reduction of 4-nitrophenol, and improvement of antibacterial behavior. The growth inhibition activity of Ag/CFO NPs was observed against *Pseudomonas aeruginosa* (18.18 ± 2.48 mm) and *Staphylococcus aureus* (10.14 ± 0.72 mm). Furthermore, Ag/CFO NPs displayed good reusability after three consecutive runs. Therefore, Ag/CFO material is shown to be a potential multifunctional catalyst in wastewater treatment.

1. Introduction

It is well recognized that advanced oxidation processes (AOPs) are a very efficient technique, particularly for removing dyes from aqueous environments. Statistics on the number of publications about AOPs from 2009 to 2019 show a consistent rise over time.[1] AOPs are typically performed between activators (such as UV radiation, transition metals, heat, microwaves, and ultrasound) and oxidizing agents (such as H_2O_2, persulfate ions, and O_3).[2] The sulfate radical has a greater oxidation potential than other oxidants, ranging from 2.5 to 3.1 V, and its active zone has a pH between 2.0 and 8.0. The sulfate radical ($SO_4^{\cdot-}$) has a half-life of 30–40 μs and is extremely stable and selective.[3] Similar to H_2O_2, the peroxymonosulfate (PMS, HSO_5^-) or persulfate (PS, $S_2O_8^{2-}$) molecules break the O–O bond when heated, illuminated, or excited by transition metals like Fe^{2+}, Cu^{2+}, Co^{2+}, Ag^+, and Mn^{2+}.[2,3]

The activation mechanism of PS/PMS is still distinct from that of H_2O_2: (i) PS/PMS is easier to photodissociate than H_2O_2 under UVA and UVB irradiation conditions;[2] (ii) PS/PMS is also more easily activated by catalysts containing the elements Cu and Co; however, catalysts containing Cu and Co are more easily washed away than catalysts containing iron in an acidic environment, even under neutral conditions; (iii) in addition to producing $SO_4^{\cdot-}$, the PS/PMS activation process also produces O_2, which is particularly common for PS and is infrequently observed during H_2O_2 activation. Spinel, valency transition metals, transition metal oxides, metal-based on carbon, and optically supported semiconductors are examples of catalysts that can be utilized to activate PS/PMS.[2,3]

Recovering the utilized catalysts from the water treatment process is a huge challenge. Therefore, magnetic field-assisted separation is suggested as one approach. Recent years have seen increasing research on magnetic materials, especially spinel ferrite materials.[3] The spinel ferrite materials commonly used to remove pollutants through AOPs are $CoFe_2O_4$, $MnFe_2O_4$, $NiFe_2O_4$, $CuFe_2O_4$, and $ZnFe_2O_4$.[3] Due to high PMS activation efficiency and outstanding magnetic properties, $CoFe_2O_4$ demonstrates potential as an appropriate candidate for the cleaning of pollutants.[4]

Dangerous bacteria such as *Escherichia coli*, *Salmonella enterica*, *Pseudomonas aeruginosa* (*P. aeruginosa*), *Listeria monocytogenes*, *Staphylococcus aureus* (*S. aureus*), and *Enterococcus faecalis* always appear in the environment, especially in the

ᵃFaculty of Materials Science and Technology, University of Science, VNU-HCM, 700000, Vietnam. E-mail: lvhieu@hcmus.edu.vn

ᵇVietnam National University Ho Chi Minh City, 700000, Vietnam

ᶜLaboratory of Multifunctional Materials, University of Science, VNU-HCM, 700000, Vietnam

ᵈCenter for Innovative Materials and Architectures, VNU-HCM, Ho Chi Minh City, 700000, Vietnam

† These authors contributed equally to this work.

water environment.[5] $CoFe_2O_4$ is known as a good dye treatment catalyst, but it is not impressive for the antibacterial activity rather to other nanometals such as nano-Ag, Au, and Cu; among them, silver nanoparticles (Ag NPs), one of the most common nanomaterials, can kill various microorganisms.[6] Additionally, it was discovered that the antibacterial activity of the Ag coated on $CoFe_2O_4$ nanocomposite is superior to that of Ag NPs.[7] Besides, $Ag/CoFe_2O_4$ materials were synthesized by Feng X. *et al.* applying the photoreduction method, and the Ag content was achieved in the material at 1.7%.[8] The methylene blue (MB) decomposition efficiency was 96.3% after 30 min under halogen tungsten irradiation (0.1 g L^{-1} 1.7% $Ag/CoFe_2O_4$ and 0.1 g L^{-1} PMS). $Ag/CoFe_2O_4$ has a catalytic efficiency that is 3.8 times greater than $CoFe_2O_4$. Thus, $Ag/CoFe_2O_4$ nanoparticles (Ag/CFO NPs) composite is promising for dye, organic chemical, and bacteria treatment in actual wastewater.

To synthesize Ag NPs, various plant extracts have been utilized as reducing agents.[9-14] This method is an eco-friendly, green, nontoxic, cost-effective, low-temperature, large-scale, and simple approach for synthesizing metal.[15] Besides, plants are a renewable and fast-recovering source of biomass. Moreover, tea's antioxidant properties are strongly connected ($R^2 = 0.81$) with the total polyphenol content of tea infusions.[16] Phenolic acids, coumarins, flavonoids, stilbenes, and lignans are all examples of polyphenols. There are also other polymerized forms like tannins and lignins.[17] Previous studies have shown that polyphenols can reduce metal ions.[10,18-20] A typical mechanism can be found in the research of Omidi S. *et al.* (2018).[21] Among the plants, jasmine flower tea contains high polyphenol components.[16] Jasmine has been shown to have the highest antioxidant and anticancer effects among plants such as blueberry, pomegranate, mango, mint, peach, and lemon.[22] Additionally, the development of Au NPs provided evidence of jasmine tea's excellent antioxidant activity compared with green tea, black tea, and orange juice.[23] Besides, jasmine is one of the most popular and easy-to-find plants. Jasmine extract has been used in prior research to fabricate Ag NPs and palladium NPs.[15,24] Nowadays, some studies have reported Ag NPs combined with metal oxide using plant extract as a reducing regent. For example, Gingasu D. *et al.* successfully synthesized $CoFe_2O_4$–Ag nanoparticles using hibiscus flowers and leaves in which the polyphenols in plant extract act as a reducing agent.[11] The study demonstrated that the saturation magnetization value (M_s) of the $CoFe_2O_4$–Ag material synthesized from hibiscus flower extract is greater and more superparamagnetic than that of the sample synthesized from hibiscus leaves. Additionally, Gram-negative (*Escherichia coli*), Gram-positive (*Enterococcus faecalis*), and yeast (*Candida albicans*) strains are all susceptible to $CoFe_2O_4$–Ag material's antibacterial activity.

According to prior studies, Ag/magnetic oxide materials have very few applications per material in the water treatment fields.[8,25-27] To strive towards the simultaneous treatment of dyes, 4-nitrophenol, and bacteria simultaneously in water, a magnetically recoverable multifunctional Ag/CFO NPs was created in this study. In this work, Ag/CFO NPs were fabricated in two steps: (i) synthesis of $CoFe_2O_4$ nanoparticles (CFO NPs) by hydrothermal technique, (ii) reduction of Ag^+ ions to Ag^o by using jasmine extract as a reduction agent. According to our knowledge, this study is the first to fabricate Ag/CFO NPs using jasmine extract as a reducing agent for Ag^+ ions. This approach is more eco-friendly, non-toxic, and cost-effective than previous studies.[8,28] Experiments to investigate the catalytic activity of dye (MB, methyl orange (MO), and rhodamine B (RhB)) and 4-nitrophenol (4-NP) degradation, and antibacterial were carried out. The chemical structure of MB, MO, RhB, and 4-NP are shown in Fig. 1. Besides, due to the magnetic properties, Ag/CFO NPs separated from the aqueous solution *via* a magnet. Thus, Ag/CFO composite is a potential candidate for actual wastewater treatment.

2. Experimental

2.1. Materials

Cobalt nitrate hexahydrate ($Co(NO_3)_2 \cdot 6H_2O$), iron(III) chloride hexahydrate ($FeCl_3 \cdot 6H_2O$), sodium hydroxide (NaOH), silver nitrate ($AgNO_3$), MO ($C_{14}H_{14}N_3NaO_3S$), and MB ($C_{16}H_{18}N_3SCl$) were purchased from Xilong, China. Oxone (PMS), RhB ($C_{28}H_{31}ClN_2O_3$), sodium borohydride ($NaBH_4$), and 4-NP were purchased from Sigma-Aldrich. Jasmine flowers were collected in Vietnam. The chemicals are utilized without undergoing any additional purification procedures.

2.2. Preparation of CFO NPs

$CoFe_2O_4$ NPs were fabricated by a hydrothermal technique following our previous reports.[31] The hydrothermal system was chilled to ambient temperature after the reaction period was completed. After the process, the solid was separated and repeatedly cleaned using ethanol and deionized (DI) water. Then, the solid was dried at 90 °C, and black powders were obtained.

2.3. Preparation of Ag/CFO NPs

Ag/CFO NPs have been fabricated by the chemical reduction method. First, 100 mL of DI water was added and continuously stirred with 4.0 g of dried jasmine flowers at 80 °C for 2 h. After that, a yellowish jasmine solution was obtained using Newstar filter paper ($\phi = 110$ mm, pore size 20–25 μm). The jasmine extract solution acted as a reducing solution in the production of silver nanoparticles based on the CFO sample (Fig. 2). Second, a mixture was prepared by adding 0.15 g of CFO NPs to 100 mL of DI water, followed by sonication for 30 min. Next, 50 mL $AgNO_3$ solution (3×10^{-3} g mL^{-1}) was dropped into the above mixture, and mechanically agitated for 30 min. Following that, 20 mL of the jasmine solution was added to the mentioned above system and mechanically agitated continuously for 3 h at 80 °C. For collecting Ag/CFO, the solid was separated, washed with DI water and ethanol, then dried at 60 °C.

2.4. Characteristics

X-ray powder diffraction (XRD) (D2 PHASER, Bruker, Germany) ($\lambda_{Cu\ K\alpha} = 1.54056$ Å) was used to determine the crystalline size and phase content of samples in the 2θ range of 10–80° at a scan rate of 0.02° min^{-1}. Fourier-transform infrared (FT-IR) spectra
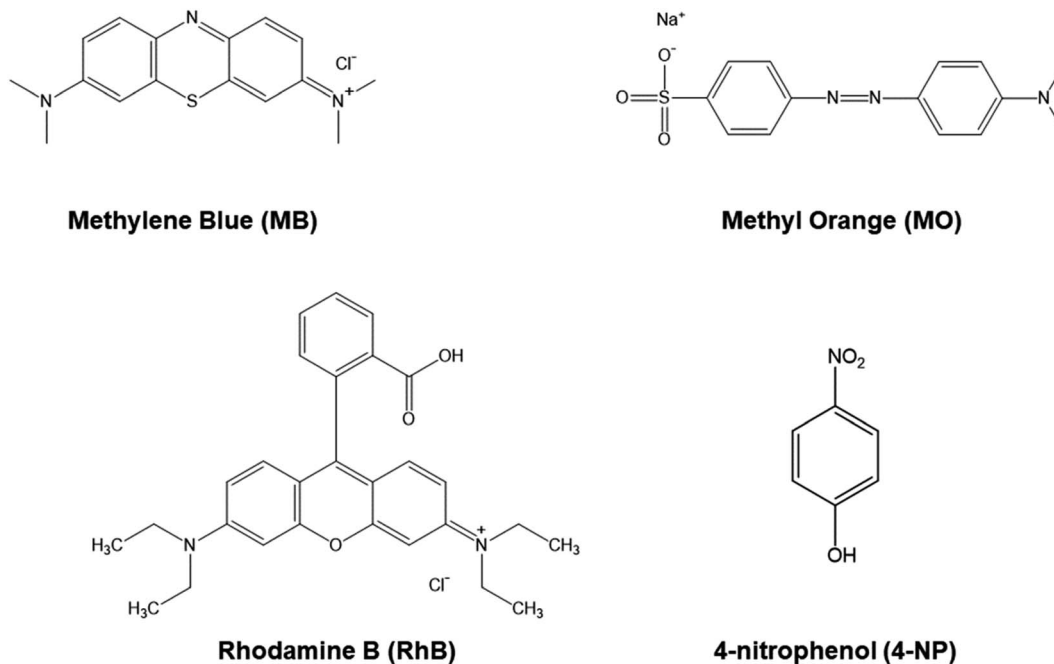
Fig. 1 The chemical structure of MB, MO, RhB, and 4-NP.[29,30]

were measured from 4000 to 400 cm^{-1} using Nicolet 6700 (Thermo Fisher Scientific, USA) and the KBr disk method. The structural morphologies of samples were characterized by field-emission scanning electron microscopy (FE-SEM) using an S-4800 device (HITACHI, Japan) at an acceleration voltage of 10.0 kV and at room temperature. The elemental content present on the surface was analyzed by energy-dispersive X-ray (EDX) spectroscopy, using the EMAX ENERGY system combined with the S–4800 device. Elemental analysis measurements were carried out on an Agilent Technologies 7800 inductively coupled plasma mass spectroscopy (ICP-MS). Vibrating sample magnetometry (VSM) (System ID: EV11, SN: 2010062, Japan) was used to evaluate the magnetic characteristics of the samples with an applied magnetic field in the range −12,000–+12 000 Oe.
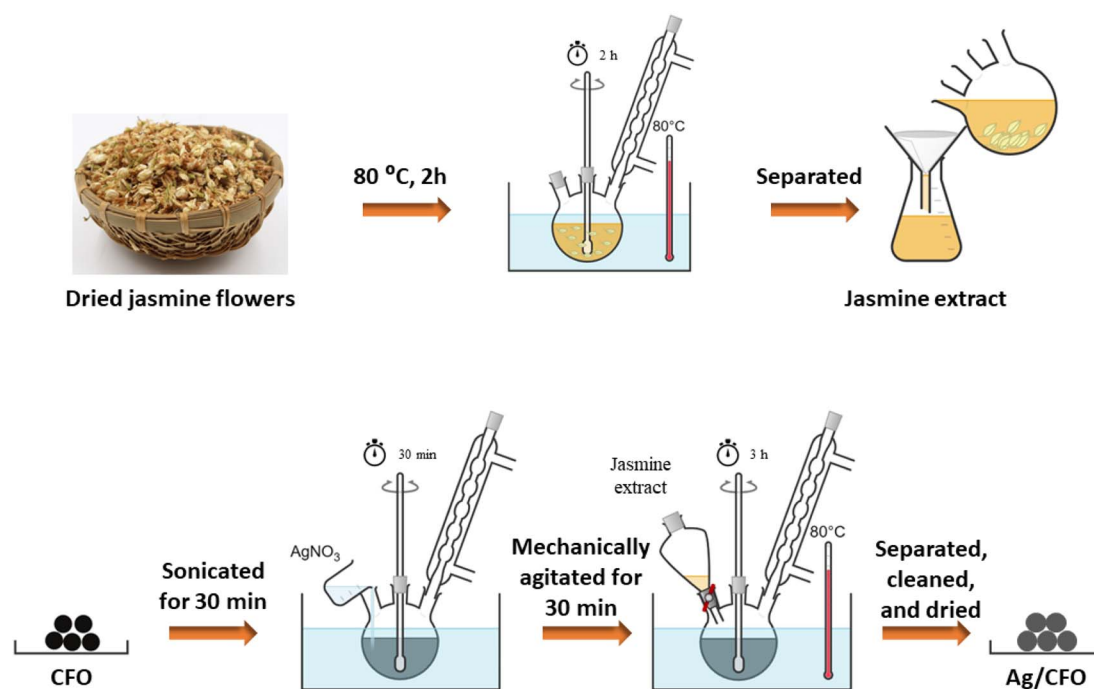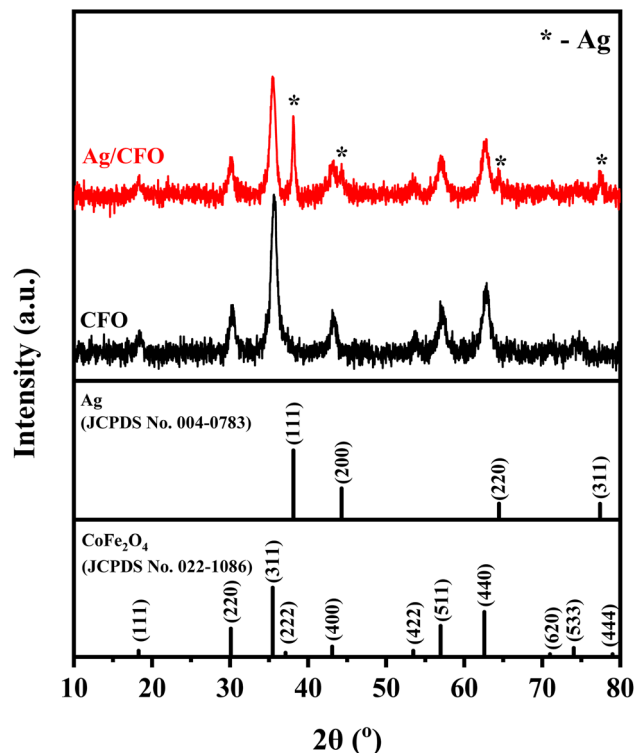

Fig. 2 The synthesis process of Ag/CFO nanoparticles.

Fig. 3 XRD patterns of CFO and Ag/CFO NPs.

Fig. 5 FT-IR spectra of CFO and Ag/CFO NPs.

2.5. The catalytic activity test of 4-NP decomposition

A quartz cuvette was filled with 0.1 mL 4-NP 0.005 mol L^{-1}, 2 mL DI water, and 1 mL NaBH$_4$ 0.2 mol L^{-1}. Then, pour 60 μL of catalyst (2 mg mL^{-1}) into the cuvette containing the above-mentioned mixture. The catalyst was taken out from the solution using a magnet after a determined time. UV-vis absorption
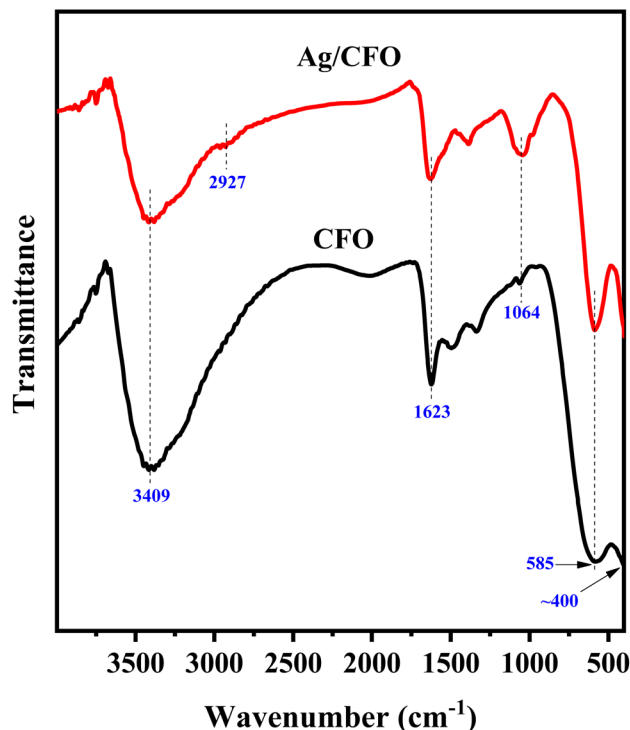
spectroscopy (250–600 nm) measured the solution after removing the catalyst.

2.6. The catalytic activity test of dyes (MB, MO, and RhB) decomposition

0.1 g L^{-1} of catalyst was added into 250 mL of a 10 ppm dye solution using a mechanical stirrer and equilibrated
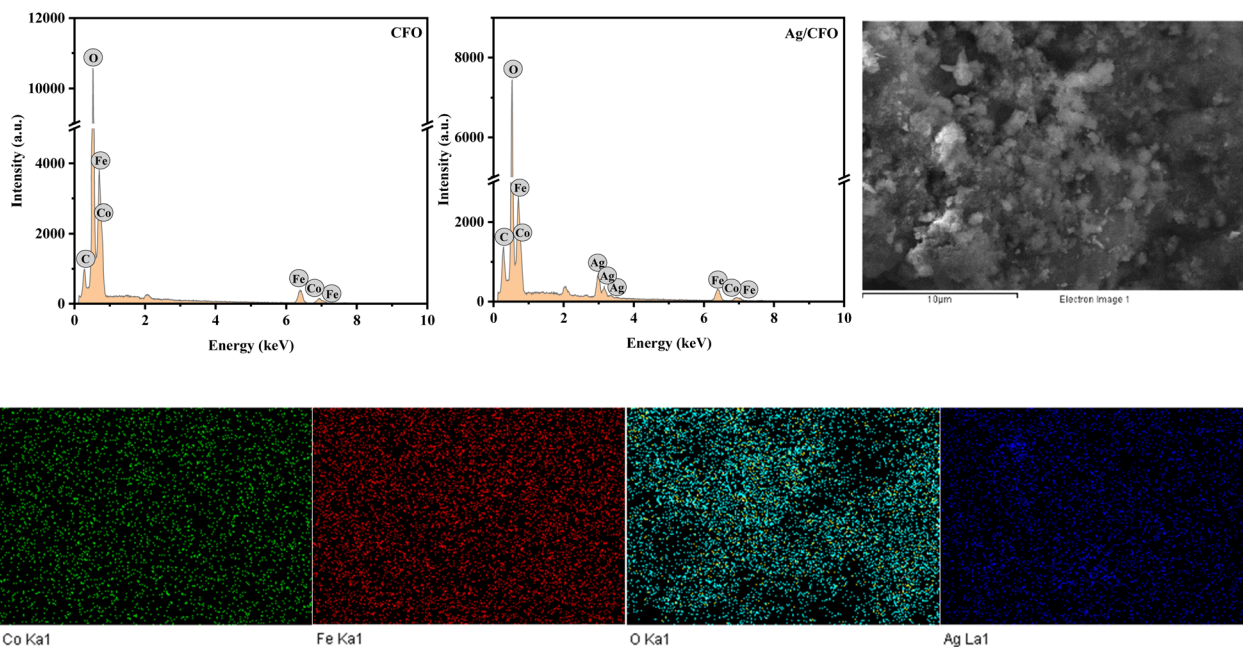

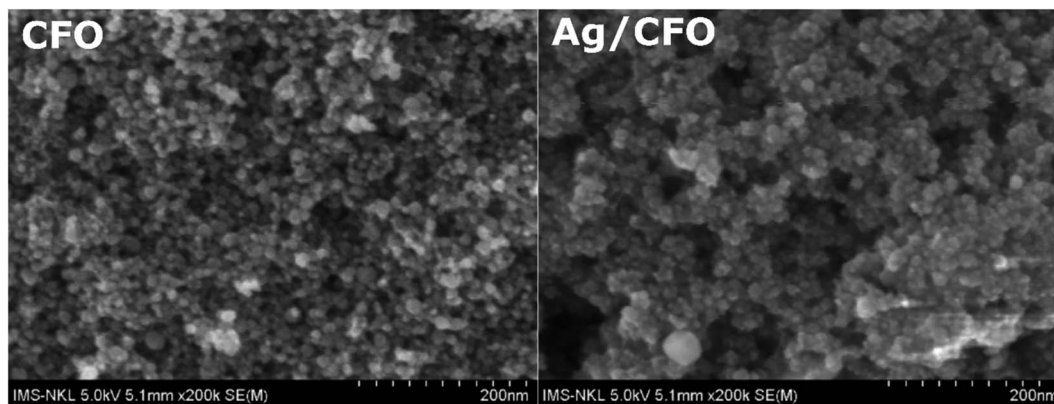**Fig. 4** EDX spectra of samples and EDX mappings of Ag/CFO NPs.

Fig. 6 FE-SEM images of CFO and Ag/CFO NPs.

adsorption–desorption for 60 minutes. The mixture above was added 0.1 g L^{-1} PMS and stirred continuously for an additional 60 minutes. 10 mL of the mixture was taken out of the system every five minutes, and a magnet was used to separate the catalyst from the solution. The optical density of dye solutions was measured at a typical wavelength using a visible spectrometer V-5100.

2.7. Recycle test

A recycling experiment was designed to evaluate the catalyst's suitability for reuse after recovery. After the reaction, the Ag/CFO NPs were magnetically separated, rinsed three times with DI water and ethanol, and dried at 60 °C until their mass remained unchanged. Similar procedures were performed three times.

3. Results & discussion

Fig. 3 is the XRD diagram of the CFO and Ag/CFO samples. The presence of characteristic diffraction peaks of CFO was observed in both samples. The peaks at $2\theta = 18.3°$, 30.1°, 35.5°, 37.1°, 43.1°, 53.5°, 57.0°, 62.6°, and 74.0° corresponding to the (111), (220), (311), (222), (400), (422), (511), (440) and (533) lattice planes (JCPDS No. 022-1086), respectively. The face-centered cubic crystal structure of Ag (JCPDS No. 004-0783) found in the Ag/CFO sample has the diffraction peaks of Ag at $2\theta = 38.1°$, 44.3°, 64.4°, and 77.5° corresponding to the (111), (200), (220), and (311) lattice planes, respectively. It is indicated that successfully reducing process Ag^{+} ions by a reducing and stabilizing jasmine flower agent. The phase percentages were determined using the X'Pert Highscore Plus software (Version 3.0). The Ag phase percentage in the Ag/CFO sample accounted for 4.5%.

Fig. 4 displays the EDX spectrum of the CFO and Ag/CFO samples. In the EDX spectrum of both CFO and Ag/CFO NPs, the peaks of O, Fe, and Co elements were observed. For the Ag/CFO sample, three Ag peaks appear between 2.8 and 3.5 keV in the EDX spectrum. Based on the element distribution map (EDX mapping), the atoms are pretty evenly distributed throughout the sample structure. Thus, the EDX results and the EDX
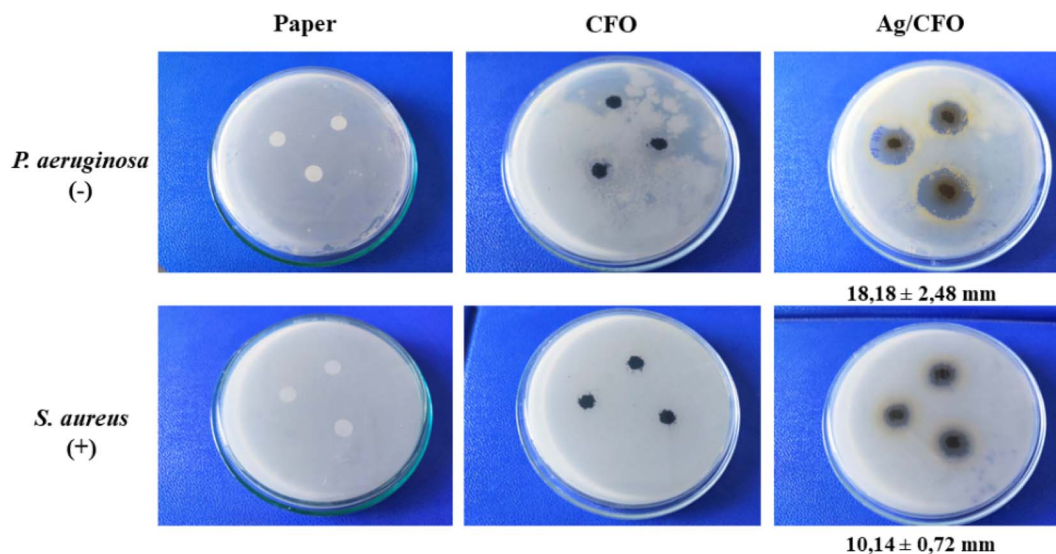

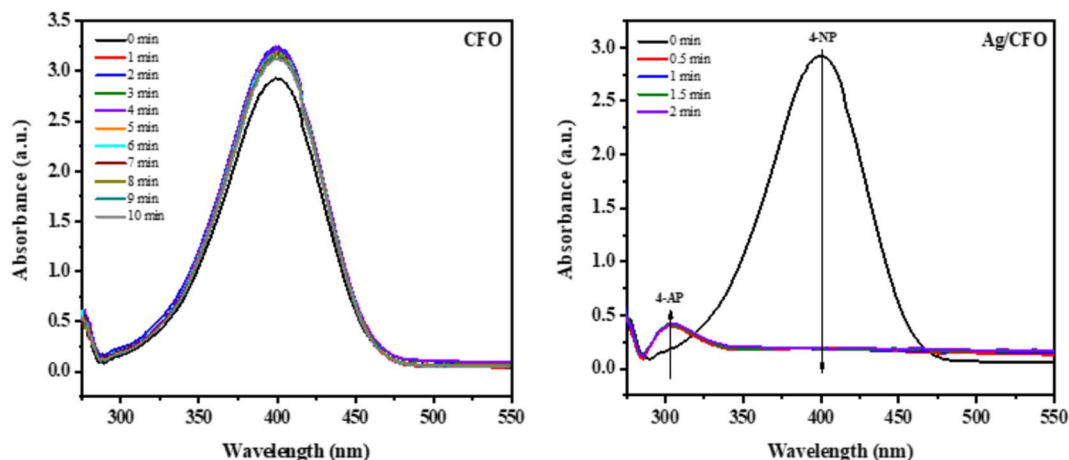Fig. 7 Antibacterial performances of CFO and Ag/CFO NPs.

Fig. 8 The UV-vis spectrum of 4-NP *vs.* time using CFO and Ag/CFO NPs.

mapping have proved the existence of elements in both CFO and Ag/CFO samples. The decorating ratio of Ag NPs over CFO NPs was found to be 0.07 wt% by the ICP-MS analyses performed on the Ag/CFO sample.

The characterized vibrations of CFO and Ag/CFO NPs are shown in FT-IR spectra (Fig. 5). The board peak in the region of 3500–3300 cm^{-1} and the peak at 1623 cm^{-1} are typical for the stretching and bending vibrations of the O–H bond of the adsorbed H_2O molecule in the sample, respectively.[32,33] The 585 cm^{-1} peak was assigned to the metal–oxygen stretching vibration in the tetrahedral sites, while the peak of about 400 cm^{-1} was assigned to the metal–oxygen stretching vibration in the octahedral sites.[32,34] The peak at 1064 cm^{-1} in the CFO sample is the stretching vibration of the Fe–Co bond and this peak intensity is enhanced in the Ag/CFO sample due to the resonance from the C–O stretching vibration of phenolic compounds in the organic chemical structure of jasmine extract.[15,35] Similarly, C_{sp3}–H bond stretching vibration was also found at 2927 cm^{-1} in the Ag/CFO sample.[15]

The surface morphology of the CFO and Ag/CFO samples is shown in Fig. 6. The FE-SEM image of the CFO sample shows that the particles are spherical and the particle size (*d*) of particles is 16.45 ± 2.52 nm. In the Ag/CFO sample, there are two different sizes of particles: small particles (*d* = 16.87 ± 2.46 nm), which may belong to CFO NPs, and large particles (*d* = 46.5 nm), which may belong to Ag NPs or Ag/CFO NPs.

The antibacterial performances of the material were investigated based on two strains of Gram-negative (*P. aeruginosa*) and Gram-positive (*S. aureus*) bacteria (Fig. 7). CFO material did not produce an antibacterial ring, while Ag/CFO material had good antibacterial properties. For the bacterial *P. aeruginosa* and *S. aureus*, the Ag/CFO material formed an antibacterial zone with diameters of 18.18 ± 2.48 mm and 10.14 ± 0.72 mm, respectively. Silver ions may be released and kill the bacteria by Ag/CFO NPs (Fig. 11d). Due to electrostatic attraction and affinity to sulfur proteins, silver ions can stick to the cell wall and cytoplasmic membrane. The order of steps is as follows: disruption of the cell wall and cytoplasmic membrane; denaturation of ribosomes; cessation of adenosine triphosphate (ATP) synthesis; membrane disruption by reactive oxygen species; interference with DNA replication; denaturation of the membrane; perforation of the membrane.[36]
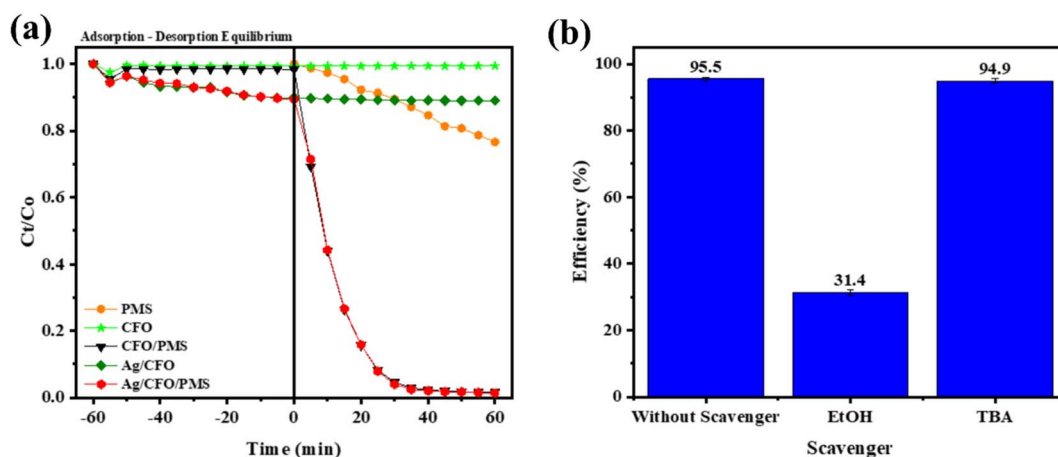

Fig. 9 (a) The degradation of MB *vs.* time of catalysts and (b) the MB removal efficiency of the CFO/PMS system.

Table 1 The catalytic activity data of the current samples are compared to those published in previous studies

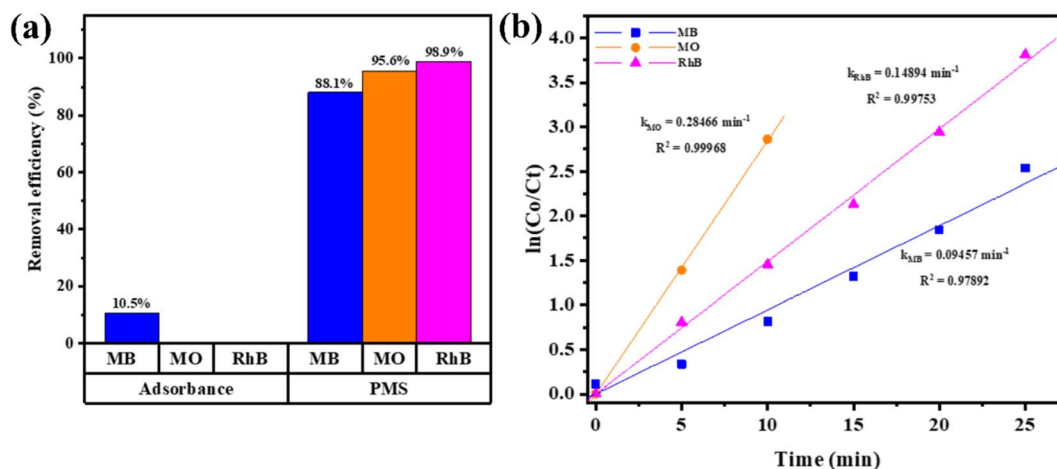| Catalysts	[Catalyst] (g L^{-1})	[PMS] (g L^{-1})	[MB] (ppm)	Light	Efficiency (%)	Time (min)	Ref.
Fe^0/Fe$_3$O$_4$/biochar	0.3	0.4	20	—	99.9	60	45
CoFe$_2$O$_4$/rGO	0.2	1.0	10	—	100	20	46
CoFe$_2$O$_4$-ZIF8	0.04	0.3	20	—	97.9	60	42
CoFe$_2$O$_4$	0.1	0.1	10	Halogen tungsten	57.4	30	8
Ag/CoFe$_2$O$_4$	0.1	0.1	10	Halogen tungsten	96.3	30	
CFO	0.1	0.1	10	Dark	93.9	30	This work
Ag/CFO	0.1	0.1	10	Dark	85.5	30	

The UV-Vis spectra of the 4-NP solution were investigated *vs.* time in the reduction reaction with NaBH$_4$ corresponding to each catalyst (Fig. 8). The results show that the 4-NP reduction activity is highly effective ($H = 100\%$ after 30 s) when using Ag/CFO catalyst. Simultaneously, a new absorption peak at 302 nm of 4-aminophenol (4-AP) appeared[37,38] and increased *vs.* reaction time. Meanwhile, the 4-NP reduction efficiency of the CFO sample is very low and there is no disappearance of the new absorption peak. This result has shown the role of Ag in the Ag/CFO sample to reduce 4-NP. The 4-NP reduction efficiency, which reaches 100% within 30 s, is better than in previous studies on Ag NPs synthesized by plant extracts.[37,39–41] The mechanism for reducing 4-NP is shown in Fig. 11b. In the reaction system, 4-NP and NaBH$_4$ react to generate the 4-nitrophenolate ion. Then, the hydrogen atoms from BH$_4^-$ ions and the 4-nitrophenolate ions are adsorbed onto the catalyst surface. –NO$_2$ group of 4-nitrophenolate is attacked by these adsorbed hydrogens, which causes a reduction to 4-AP.

The adsorption and oxidation activities of the samples are shown in Fig. 9a. The adsorption efficiency for MB dyes by CFO materials is 1.6% in 60 min. Meanwhile, the Ag/CFO sample exhibited a good MB adsorption efficiency of 10.5%. In the case of the presence of PMS oxidant, both materials demonstrated good catalytic performance in the MB dye oxidation reaction. After 30 min of response, the CFO sample's efficiency was 93.9%. The CFO sample has a greater PMS activation efficiency

than Ag/CFO sample (8.4%) under the same condition. The catalytic activities of CFO and Ag/CFO in the PMS activation reaction for MB degradation were compared with previous studies in Table 1.

The free radicals produced during the oxidation reaction of dyes with PMS were determined through the use of scavengers (EtOH and TBA) (Fig. 9b). The reaction efficiency decreased when using EtOH because EtOH simultaneously traps two free radicals SO$_4^{\bullet-}$ and $^\bullet$OH.[42,43] However, TBA is an organic substance that only traps $^\bullet$OH free radicals, but the degradation efficiency was still stable.[42] Therefore, SO$_4^{\bullet-}$ radical is the main species in this system. The mechanism for the degradation of dyes is shown in Fig. 11a. The transition metal ions in CFO play a primary role in PMS activation to produce SO$_4^{\bullet-}$ radical.[3,4] For cationic dyes (MB and RhB), SO$_4^{\bullet-}$ radicals attack a positively charged atom, and then fragmented organic molecules, CO$_2$ and H$_2$O were produced. While cleavage of the azo group bridging two aromatic rings is how the degradation of MO occurs. Then, the tiny molecules keep on converting into CO$_2$ and H$_2$O.[44]

To investigate the versatility of Ag/CFO in dye treatment applications, catalytic tests were carried out with various dyes. The results are shown in Fig. 10. MO and RhB dyes are not adsorbed on the surface of Ag/CFO NPs, in contrast to MB dyes. Because metal oxide materials with –OH functional groups on their surfaces are negatively charged and MO is an anionic dye

Fig. 10 (a) The removal efficiency of dyes varies in each process after 60 min, and (b) the graph of ln(C_o/C_t) *vs.* time in the Ag/CFO/PMS system.
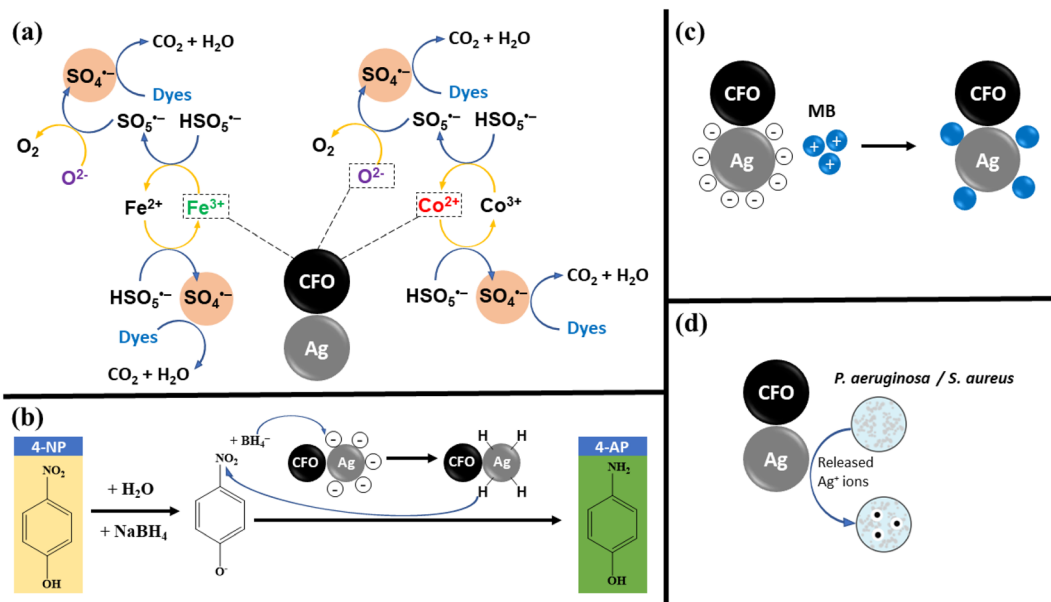
Fig. 11 The mechanism for the removal of the dyes, 4-NP, adsorption, and bacteria.
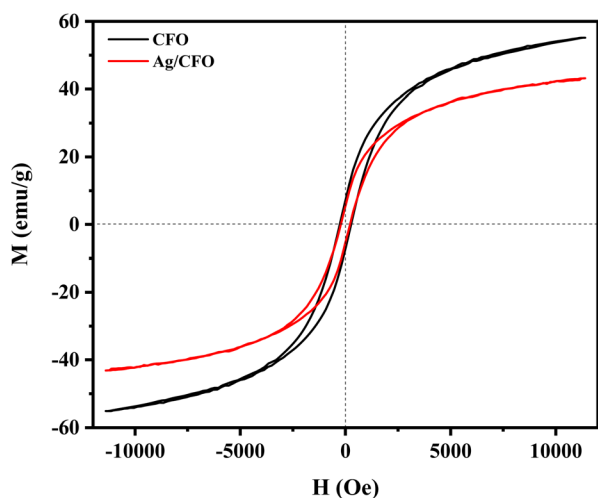

Fig. 12 M−H loops of CFO and Ag/CFO NPs.

Table 2 The magnetic values of CFO and Ag/CFO NPs

Sample	M_s (emu g^{-1})	M_r (emu g^{-1})	H_c (Oe)
CFO	55.18	7.09	277
Ag/CFO	43.11	5.35	219

that carries a negative charge, the absorbent, and the adsorbed substance were repelled from each other. However, although having a positive charge similar to that of MB, the RhB cationic dye has poor adsorption due to its bulky molecular structure, which creates a stereospecific barrier that prevents it from

adhering to the surface of the material. As a result, the best MB dye adsorption is achieved by Ag/CFO composites. However, enhancing the adsorption efficiency of Ag/CFO NPs in this study is still a challenge. Compared to previous reports, the dye adsorption performance of Ag/CFO NPs in this study needs to be improved even more in the future. The mechanism for adsorption is shown in Fig. 11c. In Fig. 10, the dye compounds that react with PMS oxidant most quickly and efficiently are displayed.

The mechanism for the removal of the dyes, 4-NP, adsorption, and bacteria is shown in Fig. 11.

Fig. 12 is the hysteresis loops of CFO and Ag/CFO samples obtained from vibration sample magnetometer (VSM) measurement. The saturation magnetization (M_s), residual magnetization (M_r), and coercivity force (H_c) values are displayed in Table 2. The M_s value of the material decreases in the presence of Ag (non-magnetic). The M_s value of 43.11 emu g^{-1} can be completely applied to recovered material after the wastewater treatment process.[47] In addition, M_r and H_c values also decrease in the Ag/CFO sample, indicating that the magnetic moments are easier to shift in the direction of the external magnetic field. Based on VSM results, Ag affected the magnetic properties of the material. Fig. 13 shows the reusability of the Ag/CFO catalyst. After three runs, RhB removal efficiency still reached 98.9%, 98.4%, and 94,5%, respectively. The decreasing active sites of metal ions cause changes in degrading efficiency during the usability study.[48] In addition, the XRD diagram and FESEM images of the Ag/CFO NPs after three runs are also shown in Fig. 13. The crystal structure and morphology of the Ag/CFO catalyst after performing three consecutive reactions remained. Thus, the above results have proved that Ag/CFO NPs have good reusability. This result promises to bring economic efficiency into practice.
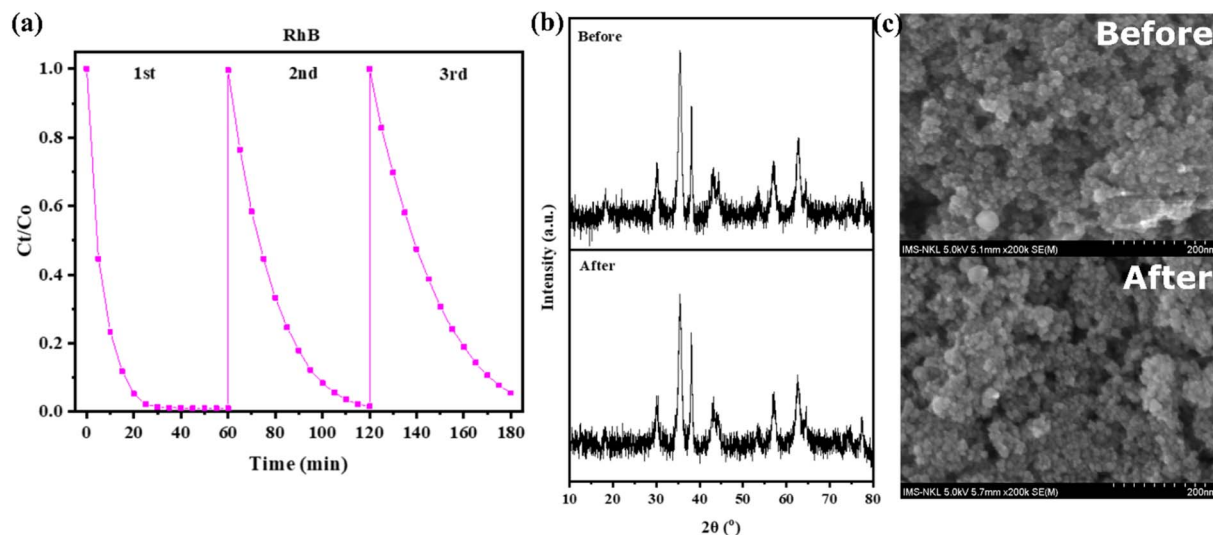
Fig. 13 (a) Reaction efficiency, (b) XRD diagram, and (c) FESEM images of Ag/CFO NPs after three runs.

4. Conclusions

In conclusion, Ag NPs were successfully decorated on CFO NPs to form Ag/CFO NPs using jasmine extract as a reducing agent of Ag^+ ions. Based on the catalytic tests, the Ag/CFO NPs can activate PMS to produce $SO_4^{\cdot-}$ radicals that degrade efficiently in different dyes in 60 min such as MB ($H = 88.1\%$, $k = 0.09457$ min^{-1}), MO ($H = 95.6\%$, $k = 0.28466$ min^{-1}), and RhB ($H = 98.9\%$, $k = 0.14894$ min^{-1}) in the non-radiation condition. Simultaneously, Ag/CFO NPs have proved more advantageous than pure CFO NPs in MB adsorption ($H = 10.5\%$), 4-NP reduction ($H = 100\%$ after 30 s), and growth inhibition activity in both *Pseudomonas aeruginosa* (18.18 ± 2.48 mm) and *Staphylococcus aureus* (10.14 ± 0.72 mm). After three recovery and reuse cycles, the Ag/CFO catalyst is still good (efficiency above 94.5% after 60 min for RhB). In summary, Ag/CFO NPs act as reusable multifunctional material and hold promise as the potential candidate in the practical wastewater treatment field.

Conflicts of interest

The authors declare that they have no known competing financial interests or personal relationships that could have appeared to influence the work reported in this paper.

Acknowledgements

References

1 H. Liu, C. Wang and G. Wang, Photocatalytic advanced oxidation processes for water treatment: Recent advances and perspective, *Chem.–Asian J.*, 2020, **15**(20), 3239–3253.

2 X. Wang, X. Zhang, Y. Zhang, Y. Wang, S.-P. Sun, W. D. Wu, *et al.*, Nanostructured semiconductor supported iron catalysts for heterogeneous photo-Fenton oxidation: a review, *J. Mater. Chem. A*, 2020, **8**(31), 15513–15546.

3 Y. Peng, H. Tang, B. Yao, X. Gao, X. Yang and Y. Zhou, Activation of peroxymonosulfate (PMS) by spinel ferrite and their composites in degradation of pollutants, *Chem. Eng. J.*, 2021, 128800.

4 Y. Ren, L. Lin, J. Ma, J. Yang, J. Feng and Z. Fan, Sulfate radicals induced from peroxymonosulfate by magnetic ferrospinel MFe_2O_4 (M= Co, Cu, Mn, and Zn) as heterogeneous catalysts in the water, *Appl. Catal., B*, 2015, **165**, 572–578.

5 B. A. Hemdan, A. M. El Nahrawy, A.-F. M. Mansour and A. B. A. Hammad, Green sol–gel synthesis of novel nanoporous copper aluminosilicate for the eradication of pathogenic microbes in drinking water and wastewater treatment, *Environ. Sci. Pollut. Res.*, 2019, **26**, 9508–9523.

6 A. Yusuf, S. Al Jitan, C. Garlisi and G. Palmisano, A review of recent and emerging antimicrobial nanomaterials in wastewater treatment applications, *Chemosphere*, 2021, **278**, 130440.

7 M. Kooti, S. Saiahi and H. Motamedi, Fabrication of silver-coated cobalt ferrite nanocomposite and the study of its antibacterial activity, *J. Magn. Magn. Mater.*, 2013, **333**, 138–143.

8 X. Feng, L. Ma, F. Cai, C. Sun and H. Ding, $Ag/CoFe_2O_4$ as a Fenton-Like Catalyst for the Degradation of Methylene Blue, *ChemistrySelect*, 2022, **7**(22), e202200237.

9 W. Elbossaty, Green tea as biological system for the synthesis of silver nanoparticles, *J. Biotechnol. Biomater.*, 2017, **7**(269), 2.

10 F. Pilaquinga, D. Amaguaña, J. Morey, M. Moncada-Basualto, J. Pozo-Martínez, C. Olea-Azar, *et al.*, Synthesis of silver nanoparticles using aqueous leaf extract of Mimosa

albida (Mimosoideae): characterization and antioxidant activity, *Materials*, 2020, **13**(3), 503.

11 D. Gingasu, I. Mindru, L. Patron, J. M. Calderon-Moreno, O. C. Mocioiu, S. Preda, *et al.*, Green synthesis methods of CoFe₂O₄ and Ag-CoFe₂O₄ nanoparticles using hibiscus extracts and their antimicrobial potential, *J. Nanomater.*, 2016, **2016**, 1–12.

12 K. Kombaiah, J. J. Vijaya, L. J. Kennedy, M. Bououdina, R. J. Ramalingam and H. A. Al-Lohedan, Okra extract-assisted green synthesis of CoFe₂O₄ nanoparticles and their optical, magnetic, and antimicrobial properties, *Mater. Chem. Phys.*, 2018, **204**, 410–419.

13 S. Khaghani and D. Ghanbari, Magnetic and photo-catalyst Fe₃O₄-Ag nanocomposite: green preparation of silver and magnetite nanoparticles by garlic extract, *J. Mater. Sci.: Mater. Electron.*, 2017, **28**(3), 2877–2886.

14 P. Laokul, V. Amornkitbamrung, S. Seraphin and S. Maensiri, Characterization and magnetic properties of nanocrystalline CuFe₂O₄, NiFe₂O₄, ZnFe₂O₄ powders prepared by the Aloe vera extract solution, *Curr. Appl. Phys.*, 2011, **11**(1), 101–108.

15 M. Aravind, A. Ahmad, I. Ahmad, M. Amalanathan, K. Naseem, S. M. M. Mary, *et al.*, Critical green routing synthesis of silver NPs using jasmine flower extract for biological activities and photocatalytical degradation of methylene blue, *J. Environ. Chem. Eng.*, 2021, **9**(1), 104877.

16 L. Gulua, L. Nikolaishvili, M. Jgenti, T. Turmanidze and G. Dzneladze, Polyphenol content, anti-lipase and antioxidant activity of teas made in Georgia, *Ann. Agric. Sci.*, 2018, **16**(3), 357–361.

17 C. Hano and D. Tungmunnithum, Plant polyphenols, more than just simple natural antioxidants: Oxidative stress, aging and age-related diseases, *Medicines*, 2020, **7**(5), 26.

18 A. Scroccarello, F. Della Pelle, L. Neri, P. Pittia and D. Compagnone, Silver and gold nanoparticles based colorimetric assays for the determination of sugars and polyphenols in apples, *Food Res. Int.*, 2019, **119**, 359–368.

19 Y. Li, Y. Chen, P. Li, G. Wang and J. Wei, Controllable deposition of Ag nanoparticles on various substrates via interfacial polyphenol reduction strategy for antibacterial application, *Colloids Surf., A*, 2022, **655**, 130287.

20 P. K. Tyagi, S. Tyagi, D. Gola, A. Arya, S. A. Ayatollahi, M. M. Alshehri, *et al.*, Ascorbic acid and polyphenols mediated green synthesis of silver nanoparticles from Tagetes erecta L. aqueous leaf extract and studied their antioxidant properties, *J. Nanomater.*, 2021, **2021**, 1–9.

21 S. Omidi, S. Sedaghat, K. Tahvildari, P. Derakhshi and F. Motiee, Biosynthesis of silver nanoparticles with adiantum capillus-veneris L leaf extract in the batch process and assessment of antibacterial activity, *Green Chem. Lett. Rev.*, 2018, **11**(4), 544–551.

22 B. Alappat, J. A. Sarna, C. Truong, K. Kleinrichert and P. Brehm, Anticancer and antioxidant properties of flavored green tea extracts, *J. Agric. Life Sci.*, 2015, **2**, 15–24.

23 Q. Liu, H. Liu, Z. Yuan, D. Wei and Y. Ye, Evaluation of antioxidant activity of chrysanthemum extracts and tea beverages by gold nanoparticles-based assay, *Colloids Surf., B*, 2012, **92**, 348–352.

24 A. Rastogi, P. Singh, F. A. Haraz and A. Barhoum, Biological synthesis of nanoparticles: An environmentally benign approach, *Fundamentals of Nanoparticles*, Elsevier, 2018. pp. 571–604.

25 S. He, C. Yang, M. Niu, D. Wei, S. Chu, M. Zhong, *et al.*, Coordination adsorption of Ag (I) on cobalt-ferrous oxalates and their derived Ag/CoFe₂O₄ for catalytic hydrogenation reactions, *Colloids Surf., A*, 2019, **583**, 124007.

26 S. Salni, M. Said, E. Eliza, A. D. D. Gayatri and P. L. Hariani, Preparation of CoFe₂O₄/SiO₂/Ag Magnetic Composite as Photocatalyst for Congo Red Dye and Antibacterial Potential, *J. Kim. Sains Apl.*, 2022, **25**(7), 235–244.

27 T. Chen, Y. Geng, H. Wan, Y. Xu, Y. Zhou, X. Kong, *et al.*, Facile preparation of Fe₃O₄/Ag/RGO reusable ternary nanocomposite and its versatile application as catalyst and antibacterial agent, *J. Alloys Compd.*, 2021, **876**, 160153.

28 S. Hara, J. Aisu, M. Kato, T. Aono, K. Sugawa, K. Takase, *et al.*, One-pot synthesis of monodisperse CoFe₂O₄@Ag core-shell nanoparticles and their characterization, *Nanoscale Res. Lett.*, 2018, **13**(1), 1–7.

29 M. Samadi, M. Zirak, A. Naseri, M. Kheirabadi, M. Ebrahimi and A. Z. Moshfegh, Design and tailoring of one-dimensional ZnO nanomaterials for photocatalytic degradation of organic dyes: a review, *Res. Chem. Intermed.*, 2019, **45**, 2197–2254.

30 Y. Zhao, P. Wang, X. Hong and K. Tang, Ni@Pd Core–Shell Nanoparticles with Tunable Comosition Supported on Glycine-Functionalized Hollow Fe₃O₄@PPy for Tandem Degradation Reduction of 4-Nitrophenol and Toxic Organic Dyes by Hydrogen Generation via Hydrolysis of NaBH₄ and NH₃BH₃, *Catal. Lett.*, 2023, 1–14.

31 A. N. Vu, N. H. T. Le, T. T. Tran, V. K. N. Nguyen, K. T. Le and H. Van Le, Preparation of magnetic CoFe₂O₄/cellulose nanocrystals composite as an catalyst for the methylene blue degradation, *J. Nat. Sci.*, 2022, **6**(2), 2064–2075.

32 M. S. Dawood, T. Elmosalami and W. Desoky, Enhancement of elastic, optical and opto-electrical properties of Ni-Substituted CoFe₂O₄ nanoparticles with different concentrations, *Opt. Mater.*, 2021, **117**, 111101.

33 T. Saravanakumar, S. Sathiya Bama, T. Selvaraju and S. Sardhar Basha, Hexacyanoferrate-complex-derived NiFe₂O₄/CoFe₂O₄ heterostructure–MWCNTs for an efficient oxygen evolution reaction, *Energy Fuels*, 2021, **35**(6), 5372–5382.

34 T. P. H. Ngo and T. K. Le, Polyethylene glycol-assisted sol-gel synthesis of magnetic CoFe₂O₄ powder as photo-Fenton catalysts in the presence of oxalic acid, *J. Sol-Gel Sci. Technol.*, 2018, **88**(1), 211–219.

35 D. Karthickraja, S. Karthi, G. Kumar, D. Sardar, G. Dannangoda, K. Martirosyan, *et al.*, Fabrication of core–shell CoFe₂O₄@HAp nanoparticles: a novel magnetic platform for biomedical applications, *New J. Chem.*, 2019, **43**(34), 13584–13593.

36 I. X. Yin, J. Zhang, I. S. Zhao, M. L. Mei, Q. Li and C. H. Chu, The antibacterial mechanism of silver nanoparticles and its application in dentistry, *Int. J. Nanomed.*, 2020, 2555–2562.

37 H. Veisi, S. Azizi and P. Mohammadi, Green synthesis of the silver nanoparticles mediated by Thymbra spicata extract and its application as a heterogeneous and recyclable nanocatalyst for catalytic reduction of a variety of dyes in water, *J. Cleaner Prod.*, 2018, **170**, 1536–1543.

38 Y. Wang, P. Gao, Y. Wei, Y. Jin, S. Sun, Z. Wang, *et al.*, Silver nanoparticles decorated magnetic polymer composites (Fe_3O_4@PS@Ag) as highly efficient reusable catalyst for the degradation of 4-nitrophenol and organic dyes, *J. Environ. Manage.*, 2021, **278**, 111473.

39 M. Zarei, N. Seyedi, S. Maghsoudi, M. S. Nejad and H. Sheibani, Green synthesis of Ag nanoparticles on the modified graphene oxide using Capparis spinosa fruit extract for catalytic reduction of organic dyes, *Inorg. Chem. Commun.*, 2021, **123**, 108327.

40 J. Kaur, J. Singh and M. Rawat, An efficient and blistering reduction of 4-nitrophenol by green synthesized silver nanoparticles, *SN Appl. Sci.*, 2019, **1**, 1–6.

41 S. H. Adyani and E. Soleimani, Green synthesis of Ag/Fe_3O_4/RGO nanocomposites by Punica Granatum peel extract: Catalytic activity for reduction of organic pollutants, *Int. J. Hydrogen Energy*, 2019, **44**(5), 2711–2730.

42 K. Zhang, D. Sun, C. Ma, G. Wang, X. Dong and X. Zhang, Activation of peroxymonosulfate by $CoFe_2O_4$ loaded on metal-organic framework for the degradation of organic dye, *Chemosphere*, 2020, **241**, 125021.

43 M. Ahmad, A. L. Teel, O. S. Furman, J. I. Reed and R. J. Watts, Oxidative and reductive pathways in iron-ethylenediaminetetraacetic acid–activated persulfate systems, *J. Environ. Eng.*, 2012, **138**(4), 411–418.

44 D. Ge, Z. Zeng, M. Arowo, H. Zou, J. Chen and L. Shao, Degradation of methyl orange by ozone in the presence of ferrous and persulfate ions in a rotating packed bed, *Chemosphere*, 2016, **146**, 413–418.

45 Y. Zhang, P. Xiangshi, J. Tian, F. Li, X. Fan, L. Ma, *et al.*, Synthesis of peroxymonosulfate composite catalyst (Fe^0/Fe_3O_4/biochar) using waterworks sludge and walnut shell for degrading methylene blue, *J. Environ. Chem. Eng.*, 2021, **9**(6), 106856.

46 L. Zou, X. Xiao, C. Chu and B. Chen, Facile synthesis of porous $CoFe_2O_4$/graphene aerogel for catalyzing efficient removal of organic pollutants, *Sci. Total Environ.*, 2021, **775**, 143398.

47 V. Mahdikhah, S. Saadatkia, S. Sheibani and A. Ataie, Outstanding photocatalytic activity of $CoFe_2O_4$/rGO nanocomposite in degradation of organic dyes, *Opt. Mater.*, 2020, **108**, 110193.

48 C. Sakthivel, A. Nivetha, G. Thiruppathi, P. Sundararaj and I. Prabha, Synthesis of a multi-functionalized $NiCo_2O_4$ spinel heterostructure via the hydrothermal route for high-performance photo-electrocatalytic, anti-bacterial and eco-toxicity applications, *New J. Chem.*, 2023, **47**(2), 571–588.